JOURNAL OF MATERIALS SCIENCE 30 (1995) 4215–4225

Microstructure and mechanical characteristics of alpha-alumina-based fibres

V. LAVASTE, M. H. BERGER, A. R. BUNSELL
Centre des Materiaux de l'Ecole des Mines de Paris, BP 87.91003 Evry cedex, France
J. BESSON
CNRS URA 866, France

The high-temperature mechanical behaviour of alumina-based ceramic fibres has been investigated by the comparison of a dense pure alumina fibre, a porous pure alumina fibre and a zirconia-reinforced dense fibre. Tensile and creep tests have been conducted up to 1300 °C in air in parallel with microstructural investigations on the as-received and tested fibres. Room-temperature behaviour of the fibres is close to that of bulk materials having the same microstructure, but the fibre form allows higher failure stresses to be attained. High-temperature deformation of the three fibres is achieved by grain-boundary sliding ($\dot{\varepsilon} \propto \sigma^2$), and is accompanied by isotropic grain growth. The specific microstructures of each fibre induce differences in the creep threshold levels as a function of temperature and stress and also in creep rates and resistance to damage. Despite better resistance to creep and damage of the zirconia-reinforced fibre, alumina-based fibres are limited to applications below 1100 °C. Grain boundaries are the principal cause of mechanical degradation at high temperature with these fibres.

1. Introduction

High-performance ceramic fibres have been developed in the last decade to reinforce metals or ceramics for high-temperature use. Non-stoichiometric silicon carbide fibres are among the best known, however they are degraded by internal oxidation reactions occurring at high temperature. Considerable interest has therefore been given by the aerospace industry to the high-temperature behaviour of existing alpha-alumina-based ceramic fibres because of the high chemical stability and resistance to oxidation of monolithic alumina coupled with its high strength and stiffness. The aim of this work was to determine the deformation mechanisms and degradation processes from room temperature up to 1300 °C in air of three alumina-based fibres. The role of the microstructure on the mechanical behaviour has been investigated in a parallel study of the evolution with temperature of mechanical properties and of the microstructural modifications occurring as a function of temperature.

2. Materials

An almost pure and dense alpha-alumina fibre (FP fibre, DuPont de Nemours), has been compared to a zirconia-reinforced alpha-alumina fibre (PRD 166 fibre, DuPont), and to a porous alpha alumina fibre (Almax fibre, Mitsui Mining).

The FP fibre is composed of more than 99% alpha-alumina, has a density of 3.92 $g\,cm^{-3}$ and a diameter of 20 μm [1]. It has high stiffness but a low elongation to failure. This brittleness makes it unsuitable for weaving and, although showing initial success as a reinforcement for light alloys, production did not progress beyond the pilot plant stage and commercial production has since ceased. Nevertheless, the FP fibre represents an example of an almost pure alumina in filament form and as such allows the fundamental mechanisms in this class of fibre to be investigated.

The FP fibre was succeeded by the PRD 166 fibre in which 20 wt % zirconia had been added to increase the elongation to failure [2]. Zirconia is known to improve strength by phase transformation toughening and to limit grain growth when added to bulk alumina. The fibre has a density of 4.2 $g\,cm^{-3}$. Production of the PRD 166 fibre did not progress beyond the pilot stage and the fibre is no longer commercially available. However, the study of the fibre permits a greater understanding of the mechanisms of toughening and the enhancement of creep behaviour of alumina fibres.

The Almax fibre from Mitsui Mining is composed of almost pure alpha-alumina. It has a diameter of 10 μm, half the diameter of the FP and PRD 166 fibres, which allows Mitsui Mining to produce woven cloth from the fibre. The fibre has a lower density of 3.60 $g\,cm^{-3}$ [3] compared to the other two fibres tested.

3. Experimental procedure

Two parallel studies have been conducted in order to characterize these three fibres. The mechanical

0022–2461

behaviour of the fibres has been studied in tension at room temperature and up to 1300 °C, and in creep. The evolution of their microstructures has been followed using scanning and transmission electron microscopy. In addition, heat treatments in air at the maximum testing temperature (1300 °C) for periods of 24 h have been carried out in order to separate the effects of the temperature and the load on the microstructural changes.

3.1. Mechanical characterization

A single-fibre testing machine [4] was used for these tests. The extremities of the fibre are maintained between one fixed and one mobile grip. The mobile grip is connected to a displacement transducer and a very sensitive load transducer mounted rigidly to the chassis of the machine. An electric motor, controlled by a servo system, displaces the mobile grip to submit the fibre to the chosen load for creep tests or to the chosen displacement speed for tensile tests. An electrical resistance oven allows the fibres to be tested up to their mechanical limits as a function of temperature.

3.2. Microstructural characterization

The diameters of the fibres were calculated by image analysis of SEM pictures of polished transversal sections of a tows containing more than 1000 fibres. The external surfaces of the fibres and their fracture morphologies were observed by SEM on a PHILIPS 501 microscope and using both a Jeol 6400 F and an Hitachi S 4500 SEM equipped with field-effect guns operating at low voltages (around 1.7 kV).

The microstructures of the fibres were determined by TEM using a Philips EM 430 TEM–STEM with an acceleration voltage of 300 kV and a maximum punctual resolution of 0.23 nm. Thin foils were obtained by glancing ionized argon sputtering using a method developed elsewhere [5].

The granulometry of the fibres was quantified by image analysis of TEM images. It was necessary to manually trace these images because of the overlapping of the grey levels of the different phases in the TEM. Pictures, with a black and white contrast associated, respectively, with the zirconia and alumina, were re-recorded using a video camera to a Tracor TN 5500 image analyser. The mean projection of each grain, $\bar{L}$, and its projections perpendicular and parallel to the fibre axis, $L_\perp$ and $L_\parallel$, were then automatically calculated. The planar environment of each alumina grain has been studied by calculating the number of alumina grains ($N_{al/al}$) or zirconia grains ($N_{al/zr}$) with which it was in contact. In the same way the environment of the zirconia grains was described by $N_{zr/al}$ and $N_{zr/zr}$.

4. Results

4.1. Characterization at room temperature

4.1.1. Microstructure of the as-received fibres

The FP fibre was seen to be circular in cross-section, Fig. 1, with a diameter of 18 ± 1.4 μm and found to be

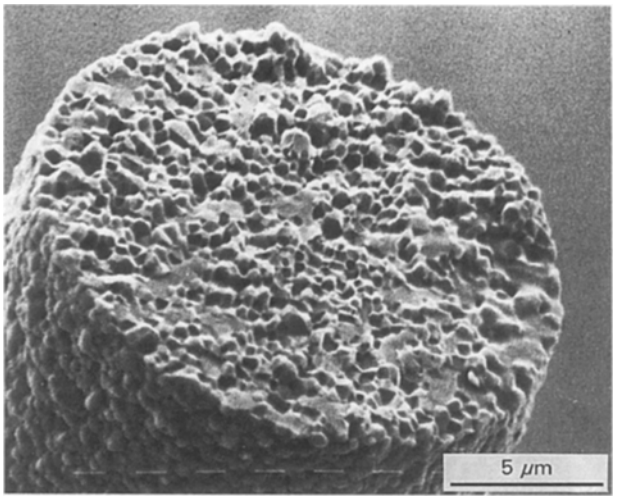

Figure 1 Scanning electron micrograph of the FP fibre failed at room temperature.

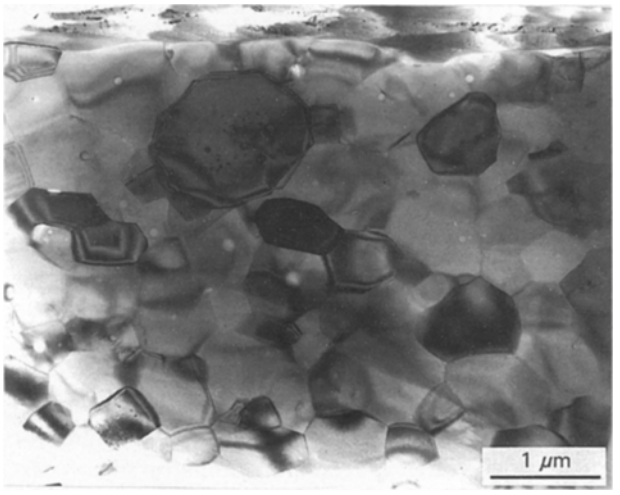

Figure 2 Transmission electron micrograph of the microstructure of the as-received FP fibre.

composed of one population of grains with a mean projection of $\langle \bar{L} \rangle = 0.50 \pm 0.25$ μm and an average of six neighbours $\langle N_{al/al} \rangle = 5.90 \pm 2.04$. The grains showed no marked preferential elongation, Fig. 2, $\langle L_\parallel / L_\perp \rangle = 1.10 \pm 0.29$ and they enclosed a small amount of small spherical porosity which could have pinned the isolated dislocations observed inside the grains. A small amount of triangular porosity was found at triple points. No obvious second phase was detected. Fresnel fringes were found at some boundaries indicating an electrical discontinuity from one grain to another which could be due to a very thin second phase, but also to a microcrack or a sputtering artefact at the grain boundary [6]. These Fresnel fringes have been encountered in the three fibres.

The PRD 166 fibre was seen to have a diameter of 17.6 ± 1.6 μm and to be composed of three populations of grains: alpha-alumina, intra- and intergranular zirconia, Figs 3 and 4. The alpha-alumina grains had a mean projection of $\langle \bar{L} \rangle = 0.34 \pm 0.18$ μm with a very slight elongation parallel to the fibre axis $\langle L_\parallel / L_\perp \rangle = 1.18 \pm 0.34$. They were surrounded by an average of three zirconia grains regularly dispersed round the alumina grains $\langle N_{al/zr} \rangle = 2.90 \pm 1.52$,

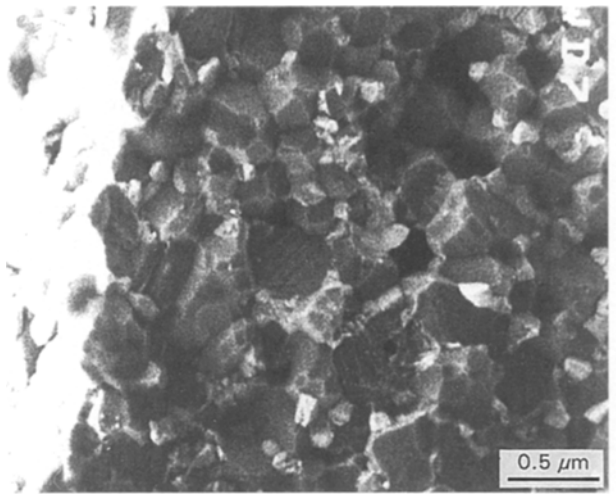

Figure 3 Scanning electron micrograph of the failure surface of the PRD 166 fibre.

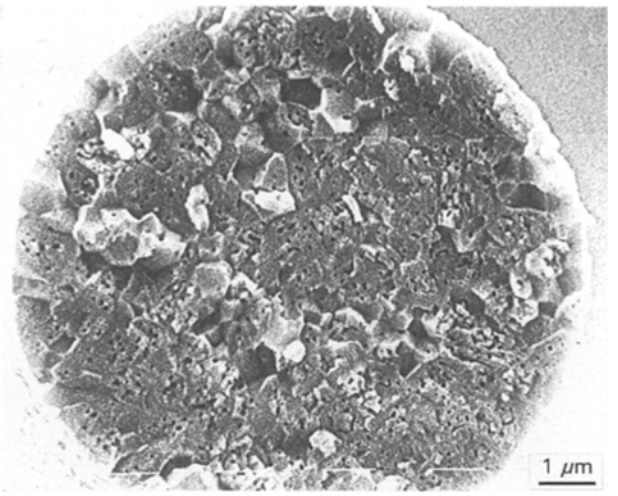

Figure 5 Scanning electron micrograph of the failure surface of the Almax fibre.

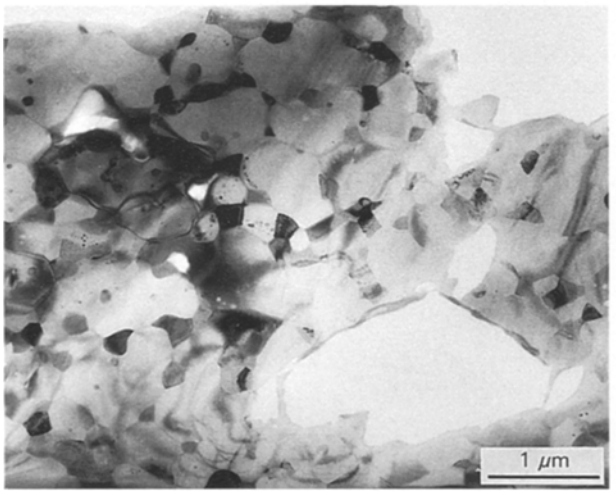

Figure 4 Transmission electron micrograph of the microstructure of the PRD 166 fibre.

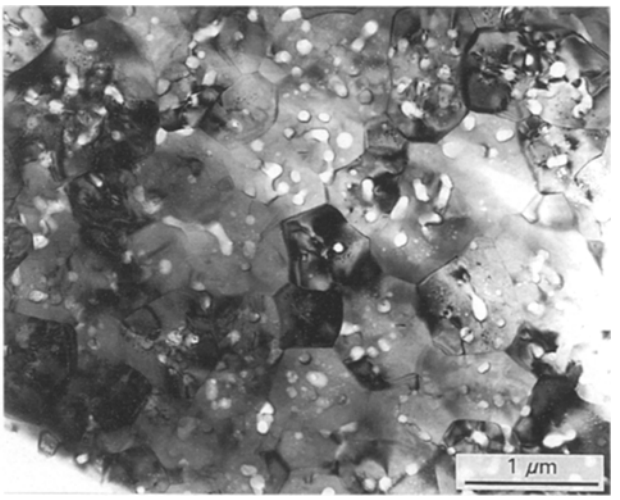

Figure 6 Transmission electron micrograph of the microstructure of the Almax fibre.

$\langle N_{al/al} \rangle = 4.55 \pm 1.65$. The alumina grains contained a small amount of porosity and zirconia particles. The size of these intragranular particles was not measured automatically, because their detection at low magnification was possible only near the Bragg position. Their size varied from a few tens of nanometres to 0.2 μm; they had circular or oval shapes with faceted interfaces and could be twinned. These intragranular particles were often grouped in elongated colonies parallel to an alumina/alumina boundary, and diffracted together with a trace of twinning which was parallel from one particle to another indicating a preferential orientation with respect to the alumina lattice. The intergranular zirconia was stabilized in its tetragonal form showing no twinning and no preferential morphological orientation $\langle \bar{L} \rangle = \langle L_{\parallel} \rangle = \langle L_{\perp} \rangle = 0.15 \pm 0.04$ μm, but was not always equiaxial, as shown by the standard deviation of the aspect ratio $\langle L_{\parallel}/L_{\perp} \rangle = 1.08 \pm 0.31$. These zirconia particles were principally located at triple points of alumina boundaries, $\langle N_{zr/al} \rangle = 3.47 \pm 1.07$, alone or grouped in pairs, $\langle N_{zr/zr} \rangle = 0.64 \pm 0.71$. No other second phase, except those producing Fresnel fringes, were clearly detected and intergranular porosity was rare.

The Almax fibre was circular in cross-section with a diameter of 9.5 ± 0.8 μm, Fig. 5, and consisted of one population of grains of around 0.5 μm mean projection, $\langle \bar{L} \rangle = 0.56 \pm 0.21$ μm, without preferential orientation, $\langle L_{\parallel}/L_{\perp} \rangle = 0.98 \pm 0.23$, each with an average of six neighbours, $\langle N_{al/al} \rangle = 6.26 \pm 2.23$, but its general appearance was completely different from the other fibres. The fibre exhibited a large amount of porosity which was essentially transgranular and associated with numerous intragranular dislocations without any periodic arrangement, Fig. 6. The diffraction contrast varied inside the same grain indicating a curvature of the grain.

4.1.2. Tensile properties at room temperature

All the fibres exhibited linear elastic behaviour with brittle failure. The failure stresses, σ_R, and failure strains, ε_R, of the three fibres are presented in Table I for a displacement speed of 0.75 mm min^{-1} and a gauge length of 150 mm.

The FP and PRD 166 failure surfaces were flat without any large apparent defects initiating failure,

TABLE I Mechanical characteristics in traction of the fibres at room temperature

	σ_R (GPa)	ε_R (%)	E (GPa)
FP	1.23 ± 0.37	0.29 ± 0.07	414
PRD 166	1.46 ± 0.30	0.40 ± 0.08	366
Almax	1.02 ± 0.39	0.30 ± 0.11	344

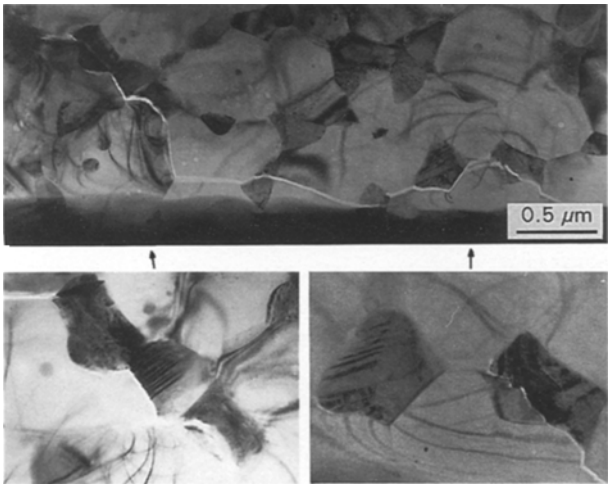

Figure 7 Transmission electron micrograph of the propagation of a crack in the PRD 166 fibre. Zirconia particles around the crack are twinned.

and the propagation mode of the crack was both inter- and intragranular, with a predominance of the intergranular mode, Figs 1, 3. The Almax failure surfaces revealed large cavities of up to 2 or 3 μm and a more pronounced intragranular propagation mode than that was seen with the other fibres, Fig. 5.

Fig. 7 shows a crack which has propagated at room temperature, during the preparation of the thin foil, inside a PRD 166 fibre which had been loaded at high temperature. The zirconia grains around the crack are twinned.

4.2. Characterization at elevated temperature

4.2.1. Tensile tests (crosshead speed of 0.75 mm min^{-1})

All the fibres exhibited linear macroscopic elastic behaviour up to 1000 °C for the FP and Almax fibres and up to 1100 °C for the PRD 166 fibre. There was seen to be a relative maximum in the failure strength at 900 °C for the FP and Almax fibre. Beyond 1000 °C, the mechanical characteristics decreased rapidly, especially for the Almax fibre, Fig. 8.

At 1300 °C, some of the PRD 166 and FP fibres tested in traction with a crosshead speed of 0.75 mm min^{-1} reached a stress plateau at approximately 0.24 GPa for both fibres. In these cases, large strains to failure were found (15%). The Almax fibre could not be adequately tested at this temperature because of its too low failure load owing to its smaller section and to the presence of defects. The Almax fibres tested at 1250 °C in tension showed the

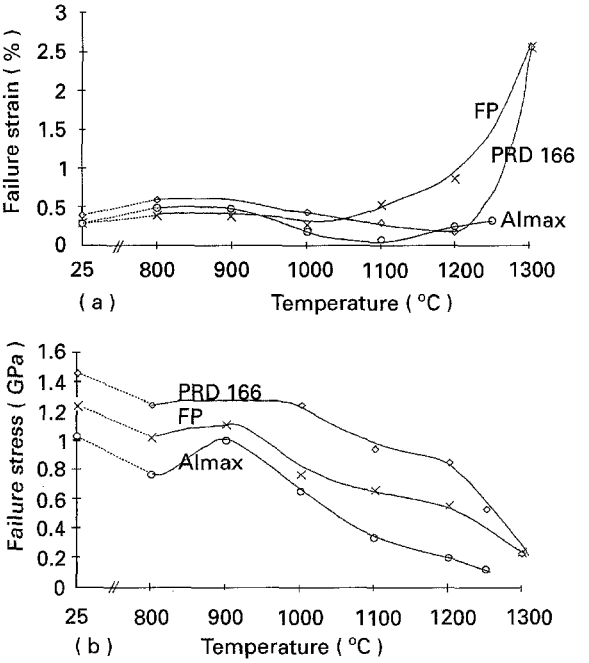

Figure 8 Evolution of (a) failure strain, (b) failure stress as a function of temperature, under tensile tests.

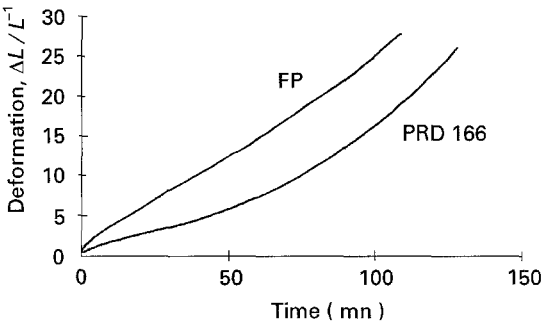

Figure 9 Examples of creep curves obtained for the FP and PRD 166 fibres at 1300 °C and 40 MPa.

beginnings of creep behaviour under 0.15 GPa with a rapid failure and small strain to failure.

4.2.2. Creep tests

No significant creep occurred below 1000 °C for the FP and Almax fibres and below 1100 °C for PRD 166 fibre. No or very little primary creep was observed above these temperatures but steady state creep was followed for the PRD 166 and FP fibres by tertiary creep which extended for longer for the PRD 166, Fig. 9. Greater time to failure and lower creep strain rates were obtained for the PRD 166 compared to the FP and also for the FP compared to the Almax fibres. Logarithmic plots of the strain rate as a function of the stress applied at the beginning of secondary creep are presented in Fig. 10 [7].

4.2.3. Microstructural evolution after heat treatment

After 24 h at 1300 °C in air with no applied load, the microstructures of the FP and PRD 166 fibres were seen to be almost stable, whereas the Almax fibre showed an isotropic grain growth of 40%,

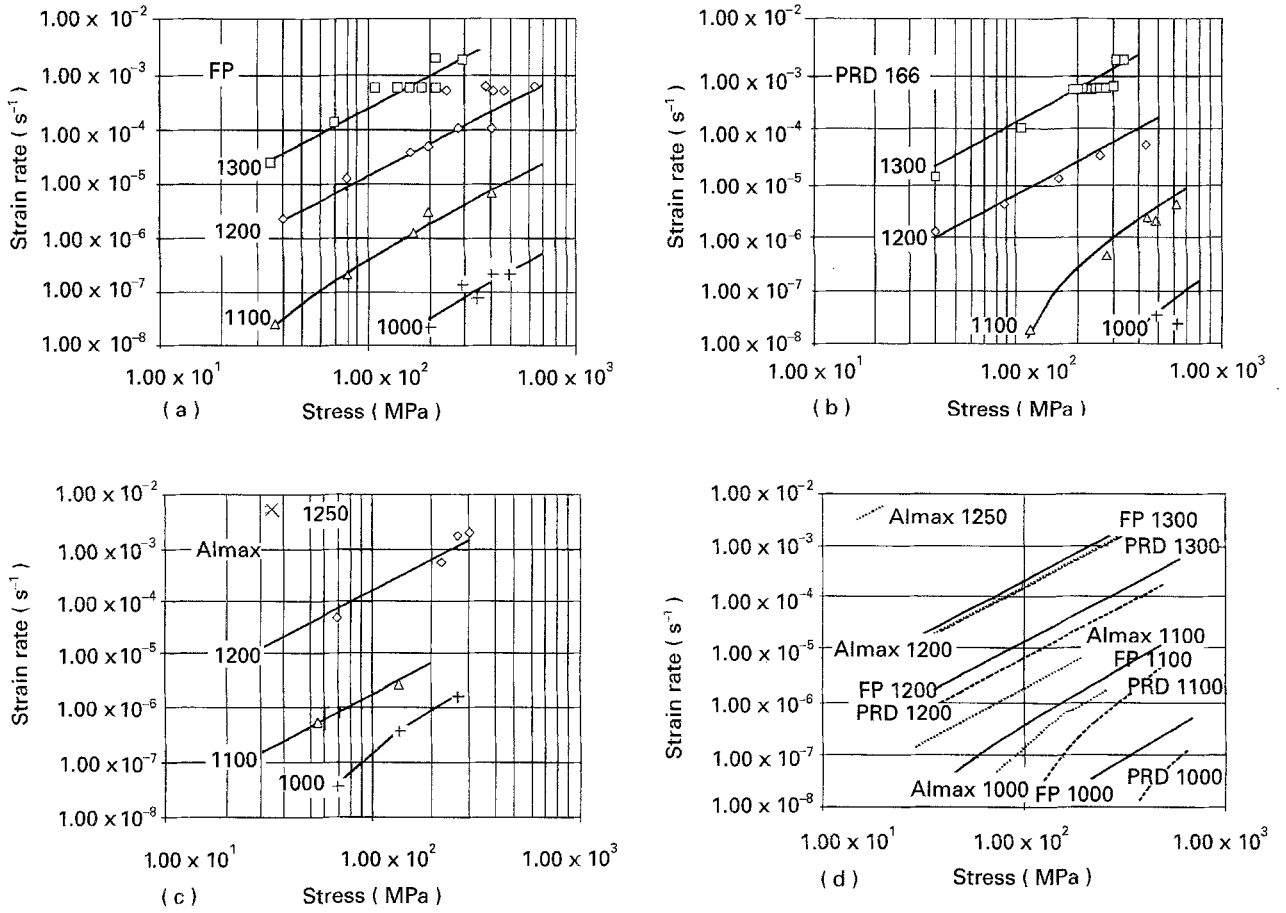

Figure 10 Logarithmic plots of the strain rates as function of the applied stresses.

$\langle \bar{L} \rangle = 0.73 \pm 0.30$ μm $\langle L_{\parallel}/L_{\perp} \rangle = 0.96 \pm 0.22$, and some relaxation of the internal stresses by a rearrangement of the intragranular dislocations into periodic networks.

4.2.4. Microstructural evolution after high-temperature loading

The microstructures of fibres loaded at high temperature were found to depend on the strain that the fibre had reached before failure. Greatest microstructural modifications were found for the largest deformations.

At 1300 °C, no significant modification of grain size was observed for a FP fibre failed with a strain of 3%, after a tensile test, whereas a grain growth of 40% ($\langle \bar{L} \rangle = 0.71 \pm 0.38$ μm) was revealed for a fibre which failed with an elongation of 30%, during a creep test, with an applied stress equal to 17% of the failure stress, Fig. 11. There was no preferential direction for the grain growth, $\langle L_{\parallel}/L_{\perp} \rangle = 1.15 \pm 0.37$ except for some isolated grains with their c-axis perpendicular to the applied load. A reduction of section of the fibre was noticed from 317 μm^2 to 272 μm^2 without any marked striction. Small triangular cavities were present at many triple points in the fibres after failure. Occasional lattice dislocations in slip bands were observed. The surface of the FP fibres broken in creep at 1300 °C after large deformations showed numerous transverse microcracks which were not observed for smaller strains, Fig. 12. The failure surfaces after creep were smoother, but not flatter, when compared to

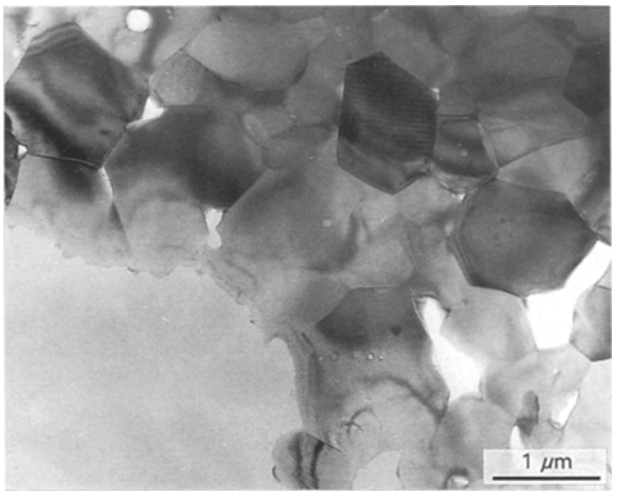

Figure 11 Transmission electron micrograph of the FP fibre after a creep failure at 1300 °C.

room-temperature failure surfaces, and become mostly intergranular, Fig. 13.

The grain growth in the PRD 166 fibre was more pronounced at 1300 °C. A 70% increase in average grain size was noticed for both alumina, $\langle \bar{L} \rangle = 0.58 \pm 0.21$ μm, and zirconia, $\langle \bar{L} \rangle = 0.25 \pm 0.07$ μm, for a fibre failed in tension at 1300 °C at a strain of 7%, Figs 14, 15. The growth was seen to be isotropic: $\langle L_{\parallel}/L_{\perp} \rangle = 1.18 \pm 0.33$ for alumina and 1.12 ± 0.32 for zirconia. No cavities were seen at triple points, but a regrouping of zirconia grains in two or threes had occurred $\langle N_{zr/zr} \rangle = 1.11 \pm 0.30$ with the appearance

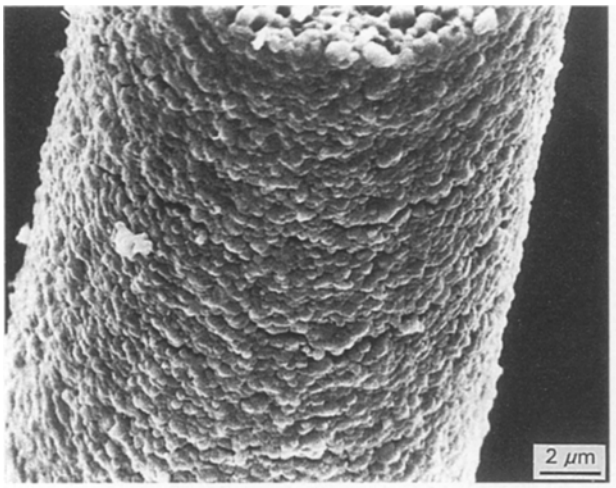

Figure 12 Scanning electron micrograph of the surface of the FP fibre broken in creep at 1300 °C at large strain. Numerous transverse microcracks can be seen to have developed.

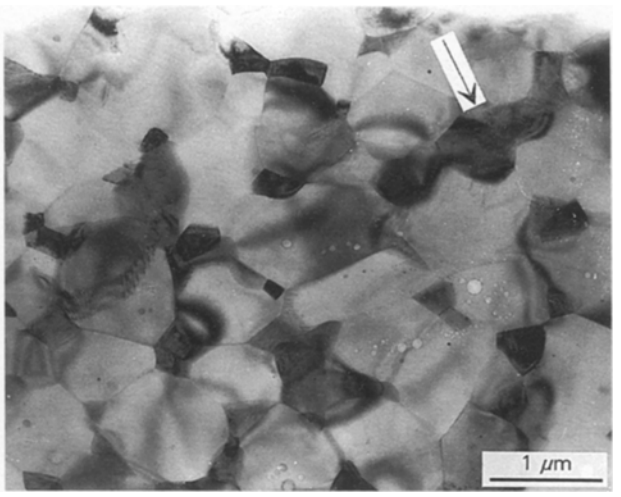

Figure 14 Transmission electron micrograph of the PRD 166 fibre after a tensile failure at 1300 °C showing grain growth and a regrouping of zirconia grains.

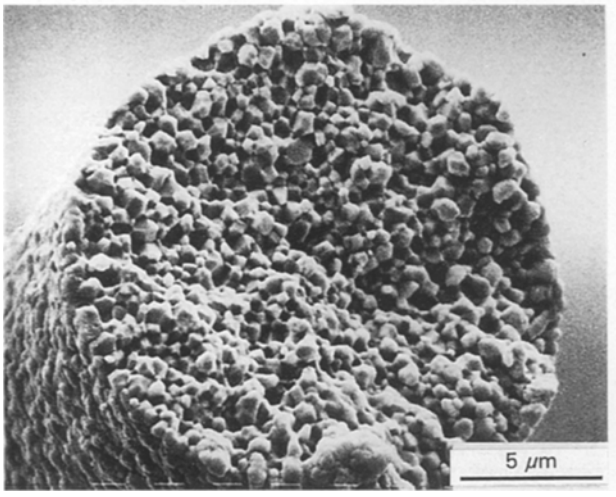

Figure 13 Scanning electron micrograph of the fracture morphology of the FP fibre tested at 1300 °C in creep.

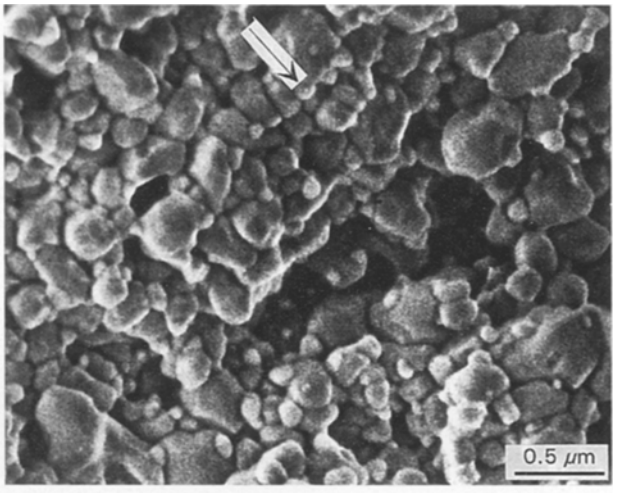

Figure 15 Scanning electron micrograph of the failure surface of the PRD 166 fibre after a creep failure at 1300 °C revealing some long chains of zirconia grains.

of some longer chains containing up to 14 grains in the thin foil section. Transverse microcracks were observed on the surface of the PRD 166 fibre, as with the FP fibre, however, to a more marked extent, and the failure became mostly intergranular, Figs 15, 16.

Tensile failure of the Almax fibre at 1250 °C revealed isotropic grain growth up to 55% $\langle \bar{L} \rangle = 0.87 \pm 0.30\ \mu m$, $\langle L_{\parallel}/L_{\perp} \rangle = 1.02 \pm 0.27$, Fig. 17. The intergranular porosity and dislocations were still present, without any relaxation of the internal stresses. Intergranular porosity was seen to be frequent under these conditions. No transverse microcracks could be observed and the failures surfaces showed the presence of large cavities, Fig. 18.

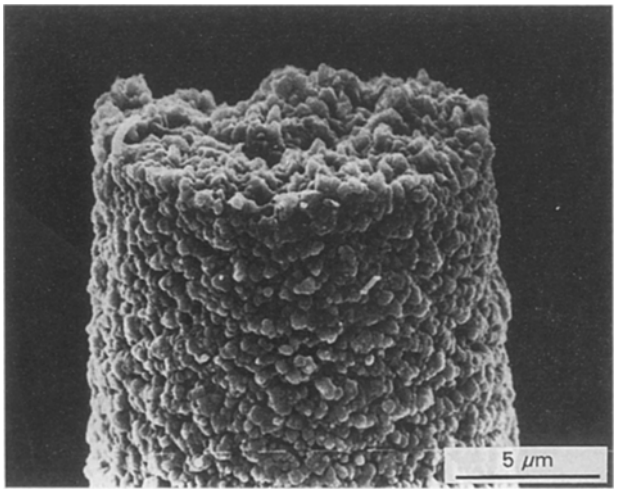

Figure 16 External surface of the PRD 166 fibre tested at 1300 °C in creep exhibiting decohesion of the grains.

5. Discussion

5.1. Behaviour at room temperature

5.1.1. FP fibre

The Young's modulus of a polycrystalline alumina depends strongly on its density, and its strength on the granulometry and the presence of flaws in the ceramic. A typical bulk alumina ceramic (10 μm grain size, a few per cent of porosity) possesses a Young's modulus of around 380 GPa and a strength of 300–400 MPa. A pure dense fine-grained bulk alumina with grain sizes of 0.5–1 μm possesses a

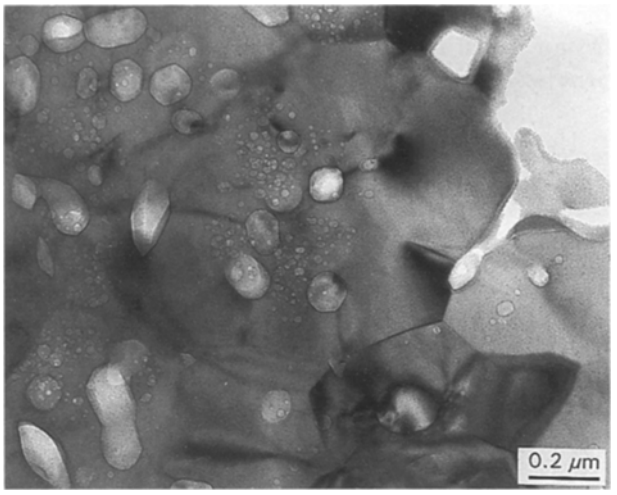

Figure 17 Transmission electron micrograph of the Almax fibre after a tensile failure at 1300 °C.

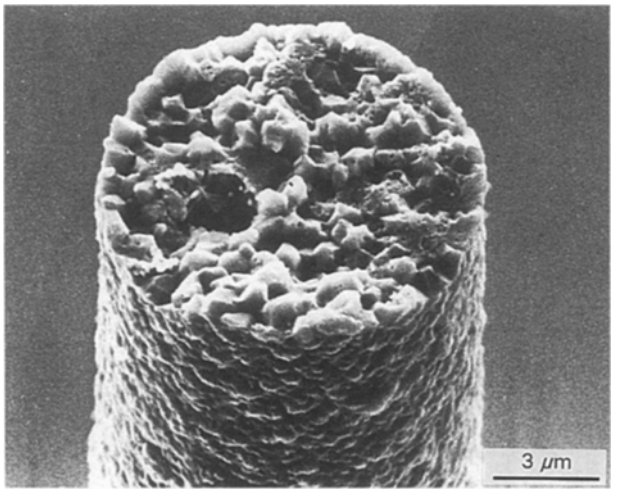

Figure 18 Fracture morphology of the Almax fibre tested at 1000 °C in traction.

strength up to 600–700 MPa and $\sigma_F/E = 0.0016$ [8, 9] giving a Young's modulus close to 440 GPa. The elastic modulus of the FP fibre is typical of dense alumina but its strength is close to twice that of the strength of a bulk material having a comparable microstructure. The room-temperature failure of fine-grained alumina is initiated by the presence of large flaws with dimensions that appreciably exceed the grain size [10]. The small cross-section which leads to the high surface/volume ratio of the fibre form lowers the probability of the presence of such large volume flaws compared to the bulk ceramic. The absence of recognizable defects on the failure surface indicates that cracks were probably initiated from a surface flaw, such as an intergranular microcrack or a large boundary. This explains why the failure stress can be increased by covering the fibre surface with a layer of silica, thus blunting the surface defects, as mentioned by Dhingra [1].

5.1.2. Almax fibre

The high porosity of the Almax, around 8%, and the presence of internal stresses, indicate a rapid grain growth of alpha-alumina grains during the fibre fabrication process. Alpha-alumina-based fibres of this type are made from the spinning of an alumina polymer precursor in which fine particles of alpha-alumina are incorporated, to avoid a porous microstructure with large grains [11]. In the FP, the granulometry of the particles incorporated was close to the final granulometry in the fibre, whereas in the Almax this granulometry was much finer, leading to rapid grain growth of both the grain issued from the precursor and from the powder, without elimination of porosity and internal stresses.

This porosity lowers the Young's modulus of the Almax fibre compared to the FP in a ratio that, for alumina [12], could be predicted by the empirical MacKenzie equation [13] which considers a fraction, P, of closed porosity of in a continuous matrix: $E_{porous}/E_{dense} = 1 - 1.9P + 0.9P^2 = 0.85 \approx E_{Almax}/E_{FP} = 344/414 = 0.83$ with $P = 0.08$. The reduction of the measured failure stress of the Almax compared to those of the FP, $\sigma_{R,Almax}/\sigma_{R,FP} = 1.02/1.23 = 0.83$, can be related to the presence in the Almax fibre, of large cavities and porosity. These defects reduce the section supporting the load from S_{tot} to S_{eff}, with $S_{eff}/S_{tot} = (D^2 - d^2)(1 - P)/D^2 = 0.84$, if $D = 10$ μm is the diameter of the fibre and $d = 3$ μm, the diameter of the large cavities. This indicates that the lower strength of the Almax fibre is not due to stress concentrations around pores but is simply due to the reduction of the cross-section. The more pronounced intragranular failure mode for this fibre shows a weakening of the grains by the intragranular porosity.

5.1.3. PRD 166 fibre

In the PRD 166 fibre, the 20 wt % (14 vol %) zirconia added is regularly dispersed at triple points of the dense alumina, pinning the movement of boundaries and hence limiting alumina grain growth: $\langle \bar{L} \rangle = 0.34 \pm 0.18$ μm for the PRD 166 fibre and 0.50 ± 0.25 μm for the FP fibre for the same initial alumina powder granulometry. Zirconia has a lower Young's modulus, $E \approx 200$ GPa, than that of alumina. The resulting elastic modulus $E = 366$ GPa of the PRD 166 is between those of a parallel configuration where the stiffness is dominated by alumina and a series configuration where the stress is equally transmitted to the two phases.

The observed increase in strength compared to the FP is due to the toughening effect of the uniform distribution of metastable tetragonal zirconia particles, which will transform around the crack tip to the monoclinic symmetry by a martinsitic reaction absorbing energy, and inducing a resulting strain in the matrix. Fracture toughness and rupture strength are thereby increased by blunting of the crack [14]. The transformed monoclinic particles can be identified on a TEM image by their twinning, when they are properly oriented with respect to the electron beam. The propagation mode of the crack for the ZrO_2 particles is more intergranular unlike that which Liang *et al.* found [15] without being "only intercrystalline", as mentioned by Rühle *et al.* [16].

5.2. Mechanism of creep deformation at high temperature

5.2.1. FP fibre

The different steady-state creep-rate laws can generally be reduced to

$$\dot{\varepsilon} = \frac{A\sigma^n}{Td^p}\exp\left(-\frac{Q}{RT}\right) \quad (1)$$

where σ is the applied stress, d the grain size, Q the activation energy for creep, n and p the stress and grain-size exponents, respectively, A is a constant depending on the material and on the mechanism controlling the deformation. The slope of the curves $\ln\dot{\varepsilon} = f(\ln\sigma)$, for a given temperature, gives a stress exponent $n = 2$. However, a slight deviation from this law is to be noted at 1100 and 1000 °C at the lower stress levels. Samples in the form of fibres with different initial grain sizes were not available to enable the grain-size exponent, p, to be determined in the classical fashion. However, grain growth accompanied high-temperature deformation, whereas no modification in grain sizes was noticed after heat treatments without applied load. The constant creep rate for a constant applied load, that occurred during an extended period could be obtained only if the reduction of section counterbalanced the increase in grain size, i.e. if S^2d^p was constant. An approximate value of $p \simeq 2$ can then be determined with the numerical values determined experimentally at the beginning and at the end of the deformation, $S_0 = 317\ \mu m^2$, $S_f = 227\ \mu m^2$, $d_0/d_f = 0.5/0.7$, by considering that the short final increase of the strain rate was only due to the damage of the fibre by the transverse microcracks which have been observed. A reduction of the strain rate for a constant applied stress due to grain growth in bulk fine-grained alumina has been reported by several authors and the grain-size exponent classically ranges from 1–3 [17–19]. The values of A and Q have been calculated by a least square fit giving $A = 50\ m^2\,K\,MPa^{-2}$ and $Q = 564\ kJ\,mol^{-1}$ [7]. The last result is in good agreement with the value of $588\ kJ\,mol^{-1}$ found by Pysher and Tressler on the FP fibres [20].

Numerous characteristics of superplastic deformation by grain-boundary sliding are found in these numerical data, such as the order of the strain rate, $\dot{\varepsilon} \approx 10^{-3}\ s^{-1}$ at 1300 °C and the stress exponent of 2, but also microstructural details such as the fine grain size, the preserved equiaxial form of the grains, strain without grain growth, observed for some samples and the presence of a small number of cavities at some triple points. Deformation by grain-boundary sliding implies some accommodation mechanisms to take up the incompatibilities which would otherwise appear at the grains surfaces [21]. If the accommodation is not sufficient, voids nucleate and grow in the grain boundary. The extended period of deformation without damage shows that a fairly good accommodation has been possible in the material.

Several accommodation mechanisms involving plastic or diffusional processes have been proposed in the literature for modelling high-temperature deformation experiments of polycrystalline alumina, depending on the grain sizes, the additives, the testing conditions, and the temperature.

The stress concentrations which develop when the sliding is hindered, can be relaxed, thanks to intragranular plasticity, by the emission of dislocations near the grain boundary [22] or inside the grain [21]. No dislocation activity in the region near the boundary has been observed which would have been implied with the core/mantle structure required for the first mechanism. A low dislocation activity has been detected within a few grains in the FP fibre after creep at 1300 °C. However, the stresses required to activate a Frank and Read dislocation source within the grain are too high compared to the threshold stress for creep, due the large Burgers vectors, imposed by the ionic structure of alumina, and due to the small length of the dislocation sources which cannot exceed the grain size of 0.5 μm. This indicates that, when basal slip has locally occurred, the source of dislocation was more probably in the adjacent boundary, as has been previously observed [23], than inside the grain. However, the low mobility of the intragranular dislocations in alumina, excludes total accommodation of the slip being achieved by intragranular plastic deformation.

The diffusion coefficient of alumina cations are lower at the grain boundaries and in fine-grained alumina, because the ratio of the grain-boundary surface to the grain volume is high enough to ensure accommodation by diffusion through these boundaries. This is not the case for large grains for which intragranular plasticity is the controlling process. A pure intergranular diffusional creep implies $\dot{\varepsilon} \propto \sigma$. In this case, the limiting process is the intergranular diffusion of aluminium cations and $Q \approx 418\ kJ\,mol^{-1} = Q_{Al^{3+}}$, the activation energy for Al^{3+} diffusion in the boundary [18]. Although this mechanism has been found in the literature, at low stresses or low strain rates [24] it is clearly not the controlling mechanism in the FP fibre, for which $n = 2$, and $Q = 564\ J\,mol^{-1} \gg Q_{Al^{3+}}$.

The diffusion process is certainly interface controlled [25], that is coupled with the glide and climb of discrete grain-boundary dislocations, the movement of which can be hindered by steps, precipitates, triple points or other defects at the boundary. The slight deviation from the σ^2 dependence of $\dot{\varepsilon}$ observed at 1100 and 1000 °C at lower stresses, could indicate that a non-negligible threshold stress, σ_0, must be attained to activate the creep. A better fit of the $\log\dot{\varepsilon} = f(\log\sigma)$ curves is possible by considering a $(\sigma - \sigma_0)^2$ dependence of $\dot{\varepsilon}$, with $\sigma_0 = 40$ MPa at 1000 °C, 15 MPa at 1100 °C and becoming negligible at higher temperatures compared to the applied stresses. However it must be noted that this result cannot be related only to the activation of grain-boundary dislocation movement as the temperature dependence of the threshold stresses, σ_0, is too great to be predicted by a dislocation climb model as this implies a linear dependence of σ_0 with the shear modulus, G [18], with $G(MPa) = 1.75 \times 10^5 - 23.4.T(K)$ [26]. Moreover, if this glide and climb process was the only limiting one,

a strain-rate variation of the form $\dot{\varepsilon} \approx M\sigma^2/d$ should be found, where M is the average mobility of the intergranular dislocations. A grain-size exponent closer to 2 indicates, however, that other steps in the accommodation could be the limiting factors. Amongst these mechanisms, triple-point fold formations [19, 27], are unlikely, as they have not been observed. Grain switching [28], grain rotation or grain formation [29] are possible. Because the results of these different accommodations cannot be distinguished when the deformation is stopped, it is hazardous to identify, from thin-foil observations, one particular controlling mechanism, and several micromechanisms certainly occur locally at the same time at different places.

Grain growth cannot be dissociated from the diffusion-controlled local transformations undergone by the grains under load, as no modification of the grain size was observed during heat treatments without load at the same temperatures. Grain growth is not directly stress-enhanced, but for it to occur the fibre has to be deformed to initiate the process. It is clear that the amount of grain growth is related to the total deformation that the structure has had to accommodate because it has only been observed for tests resulting in high strains ($\approx$30%) at 1300 °C, that is, only for low stresses but long times to failure.

The creep mechanism of the FP fibre can now be described as being based on grain-boundary sliding achieved by an intergranular movement of dislocations and accommodated by several interface-controlled diffusion mechanisms, involving boundary migration and, to some extent, by emission from the boundary of intragranular dislocations.

The failure of the fibre, at high temperature, occurred after a short period of damage, by the growth of transverse intergranular microcracks from cavities, the coalescence of which leads to an uneven failure surface. These cavities at triple points are generated by the accumulation of an array of intergranular dislocations when they are unable to pass from one boundary to another by dissociation and/or recombination. Cavities clearly are very rarely created by the pile-up of intragranular dislocations on the boundary, as cavities associated with intragranular slip bands were seldom seen. The smoother surfaces of the grains on the failure surface compared to those seen at room temperature, indicate that diffusion at the crack tip has occurred.

5.2.2. PRD 166

By comparing the FP and PRD 166 fibres the introduction of zirconia into alumina in a fibre can be seen to have improved the high-temperature mechanical properties. The PRD 166 has a better resistance to creep and damage than the FP fibre.

The improved resistance to creep of the PRD 166 fibre is indicated by an increase of temperature and stress for which creep is detected, a decrease of strain rates in the permanent regime, and the non-linearity of the $\log \dot{\varepsilon} = f(\log \sigma)$ curve at 1000 and 1100 °C. Below 1100 °C, a significant threshold stress must be reached to permit creep. From 1200 °C, the linearity of the $\log \dot{\varepsilon} = f(\log \sigma)$ curves indicates that this threshold stress can be neglected compared to the applied stresses, and a stress exponent of 2 is found. The creep law can be expressed as

$$\dot{\varepsilon} = \frac{A}{d^p T} e^{-Q/RT}[\sigma - \sigma_0(T)]^2 \qquad (2)$$

where $Q = 600\ \mathrm{kJ\,mol^{-1}}$, σ_0, the threshold stress is equal to 180 MPa at 1000 °C, 90 MPa at 1100 °C [7] and is neglected at higher temperatures. It proved impossible to estimate the exponent, p, for the PRD 166 fibre, from the evolution of $S^2 d^p$ during creep or tensile tests, as was done for the FP fibre. This was because of an earlier onset of damage in the fibre, which did not allow the separation of the effects of section reduction and the effects of damage on the increase of strain rate. A/d^p has been evaluated at the beginning of the secondary creep to be $2.13 \times 10^{15}\ \mathrm{K\,MPa^{-2}}$.

Up to 1100 °C, the introduction of dispersed particles of zirconia at triple points of grain boundaries limits the mobility of intergranular dislocations from one grain boundary to another. A threshold stress must be reached in order to allow the motion of intergranular dislocations [25] and a higher activation energy for creep is required compared to the FP fibre. From 1200 °C, the pinning of the dislocations by the zirconia grains is not sufficient to impede the thermally activated mobility of the intergranular dislocations. Moreover, the regrouping of zirconia into chains increases the ratio of triple points deprived of zirconia grains. Intergranular diffusion and motion of dislocations from one boundary to another are then facilitated, grain growth is no longer impeded, and the differences between the FP and PRD 166 creep rates decrease as temperature increases. This regrouping of the ZrO_2 grains shows that grain-boundary sliding was, in part, accommodated by grain switching in which two zirconia grains separated by an Al_2O_3/Al_2O_3 boundary move by diffusion of matter through the boundary to form a pair of zirconia grains in contact. This leads to a decrease of the surface energy of the grains by the replacement of ZrO_2/Al_2O_3 boundaries by a ZrO_2/ZrO_2 boundary. Such a regrouping of zirconia grains between alumina grains during creep is characteristic of a two-phase material in which the diffusivity of one species, here Zr^{4+}, through the boundary, is higher than the other [30].

Damage in the PRD 166 fibre, as in the FP, is produced by the formation of microcracks, due to a local lack of accommodation, which grow transversally and coalesce up to failure. A comparison of the duration of the non-linear creep regions and of the external surfaces of the fibres after a large deformation shows that damage in the FP rapidly induced failure, whereas the PRD 166 fibre resisted to higher levels of damage. Although resistant to monoclinic transformation at high temperature, the tetragonal particles toughen the fibre by deflecting the crack [31]. However, the development of dispersed microcracks

progressively decreases the load-supporting cross-section resulting in an increase in true stress at constant applied load and an increase of the strain rate.

5.2.3. Almax fibre

The Almax fibre has the lowest resistance to creep of the three fibres: the stresses at which creep is detected are lower, strain rates are higher. Creep behaviour as a function of temperature cannot be related to the classical creep models described above, even though a stress exponent of 2 is found at 1100 and 1200 °C. The times and strains to failure at each tested temperature are shorter than with the two other fibres. The correction of the $\ln \dot{\varepsilon} = f(\ln \sigma)$ curves by using the true stress supported by the matter, to take into account the porosity, allows only a small translation of the curves which is not sufficient to explain the higher strain rates. In these fibres, grain growth at 1300 °C is activated without applied load, unlike that with the other fibres, for which grain growth is a consequence of the diffusion accommodation of the slip. The intergranular porosity which appears in the fibre during creep may have been created by the interception of intragranular pores by the boundaries of the growing grains. This intergranular porosity will have grown by the absorption of vacancies that are produced at the grain boundaries during grain-boundary sliding [32]. Diffusion required to accommodate grain-boundary sliding is facilitated, and much higher strain rates are obtained. However, this intergranular pore growth, rapidly induces failure. Cannon and Coble [33] noticed this particular behaviour of bulk porous alumina during creep characterized by higher creep rate, poor fit to theoretical consecutive relations, and pore growth by diffusion.

6. Conclusion

This study has revealed the behaviour of dense, porous and reinforced alumina fibres at high temperatures and this can be summarized by a comparison of the evolution of their tensile strains and stresses to failure. The PRD 166 fibre was seen to maintain its strength to 1100 °C whereas the FP and Almax fibres lost strength at 1000 °C. This is explained by the toughening effect of zirconia in the PRD 166 fibre. The delayed increase in strain as a function of temperature of this fibre (1250 °C for PRD 166 compared to 1100 °C for FP) is due to the pinning effect of the zirconia, delaying plasticity due to boundary sliding. However, this effect is lost at 1300 °C and tensile strains are comparable. The lower failure strains and stresses of the Almax fibre are due to the presence of large flaws inside the fibre more than to its specific intragranular porosity. This porosity induces higher strain rates in creep and lower times to failure in this fibre. Failure modes, with all the fibres, become more intergranular as temperature increases due to the weakening of the boundaries, but the Almax fibre always presents a higher proportion of intragranular failure due to the porosity and internal stresses inside the grains. The blunting of the crack tip by thermally activated diffusion allows a decrease of the stress concentration around the crack tips which can be the controlling effect, in the region of 900 °C, so allowing a temporary increase in failure strength.

The modes of deformation and failure of fine-grained alumina in the fibre form are comparable with those of a bulk material. Data from pure tensile tests on bulk specimens are not numerous because of the experimental difficulty of gripping the specimens. Working on fibres allows the specimens to be gripped more easily and the development of a tensile-creep machine for single fibres with a high load sensitivity, required by the small diameter of the specimens, provides the opportunity of completing those existing studies which are available in the literature. The elastic moduli and creep behaviour at high temperature for the fibres and for the bulk materials having the same microstructures are identical. However, some differences exist which are due to the high surface to volume ratio of the fibres. Failure stresses are increased in the elastic region due to a lower bulk-defect density, but failure strains are decreased in creep due to a poorer resistance to damage.

The use of polycrystalline alumina fibres for the reinforcement of high-temperature structures is limited to 1000° and 1100 °C for zirconia-reinforced alumina. The major limitation in temperature is the presence of grain boundaries which cause, by sliding and opening, the creep and failure of the fibre. To exploit the attractive high resistance to oxidation of alumina, together with its high stiffness and the low mobility of its intragranular dislocations, grain boundaries must be avoided. This should encourage the development of small diameter monocrystalline alumina fibres.

References

1. A. K. DHINGRA, *Philos. Trans. R. Soc. Lond.* **A 294** (1980) 411.
2. J. C. ROMINE, *Ceram. Eng. Sci. Proc.* **8** (1987) 755.
3. "Almax", *commercial literature of Mitsui Mining* (1993).
4. A. R. BUNSELL, J. W. S. HEARLE and R. D. HUNTER, *J. Phys. E Sci. Instrum.* **4** (1971) 868.
5. M. H. BERGER and A. R. BUNSELL, *J. Mater. Sci. Lett.* **12** (1993) 825.
6. D. R. CLARKE, *J. Am. Ceram. Soc.* **63** (1980) 104.
7. V. LAVASTE, J. BESSON, M. H. BERGER and A. R. BUNSELL, *ibid.*, in press.
8. R. M. CANNON, in "Advances in Ceramics", Vol. 10, "Structure and properties of MgO and Al_2O_3 ceramics", edited by W. D. Kingery (American Ceramic Society, Columbus, 1984) p. 818.
9. R. W. DAVIDGE, R. C. PILLER and A. BRIGGS *et al.*, in "Technical Ceramics", edited by H. Nosbusch and I. V. Mitchell (Elsevier, 1988) p. 163.
10. A. G. EVANS and Y. FU, in "Advances in Ceramics", Vol. 10, "Structure and properties of MgO and Al_2O_3 ceramics", edited by W. D. Kingery (American Ceramic Society, Columbus, 1984) p. 697.
11. J. D. BIRCHALL, *Trans. J. Br. Ceram. Soc.* **82** (1983) 143.
12. R. L. COBLE and W. D. KINGERY, *J. Am. Ceram. Soc.* **39** (1956) 377.
13. J. K. MacKENZIE, *Proc. Phys. Soc. London* **B 63** (1950) 2.
14. F. F. LANGE, *J. Mater. Sci.* **17** (1982) 247.
15. K. M. LIANG, G. ORANGE and G. FANTOZZI, in "Proceedings of the 11th Risø International Symposium on Metallurgy and Material Science", September 1990 edited by

J. J. Bentzen, J. B. Bilde Sorensen, N. Christiansen, A. Horswell and B. Ralph (Risø National Laboratory, Roskilde, Denmark, 1990) p. 389.
16. M. RÜHLE, A. STRECKER, D. WAIDELICH and B KRAUS, in "Advances in Ceramics", Vol. 12, "Science and Technology of Zirconia II", edited by N. Claussen, M. Rühle and A.H. Heuer (American Ceramic Society, Columbus, 1984) p. 256.
17. C. CARRY, in "MRS International meeting on Advanced Materials", Vol. 7, "Superplasticity", Tokyo, May 1988, edited by M. Kobayashi and F. Wakai (Material Research Society, Pittsburg, 1989) p. 199.
18. R. M. CANNON, W. H. RHODES and A. H. HEUER, *J. Am. Ceram. Soc.* **63** (1980) 46.
19. A. H. CHOKSHI, *J. Mater. Sci.* **25** (1990) 322.
20. D. J. PYSHER and R. E. TRESSLER, *Ceram. Eng. Sci. Proc.* **8** (1987) 218.
21. T. G. LANGDON, *Philos. Mag.* **22** (1970) 689.
22. R. C. GIFKINS, *Metall. Trans.* **7A** (1976) 1225.
23. L. PRIESTER and S. LARTIGUE, *J. Eur. Ceram. Soc.* **8** (1991) 47.
24. K. R. VENKATACHARI and R. RAJ, *J. Am. Ceram. Soc.* **69** (1986) 135.
25. E. A. ARZT, M. F. ASHBY and R. A. VERRALL, *Acta Metall.* **31** (1983) 1977.
26. W. R. CANNON and T. G. LANGDON, *J. Mater. Sci.* **23** (1988) 1.
27. *Idem, ibid.* **18** (1983) 1.
28. M. F. ASHBY and R. A. VERRALL, *Acta Metall.* **21** (1973) 149.
29. R. C. GIFKINS, *J. Mater. Sci.* **13** (1978) 1926.
30. R. MARTINEZ, R. DUCLOS and J. CRAMPON, *Scripta Metall. Mater.* **24** (1990) 1979.
31. A. G. EVANS, in "Advances in Ceramics", Vol. 12, "Science and Technology of Zirconia II", edited by N. Claussen, M. Rühle and A. H. Heuer (American Ceramic Society, Columbus, 1984) p. 193.
32. J. WEERTMAN, *Metall. Trans.* **5** (1974) 1743.
33. R. M. CANNON and R. L. COBLE, in "Deformation of ceramics Materials", edited by R. C. Bradt and R. E. Tressler (Plenum Press, New York, 1975) p. 61.

Received 23 January
and accepted 22 March 1995